Monthly Notices
of the
ROYAL ASTRONOMICAL SOCIETY

MNRAS **469,** 401–415 (2017)
Advance Access publication 2017 March 30

doi:10.1093/mnras/stx800

The *Gaia* ultracool dwarf sample – I. Known L and T dwarfs and the first *Gaia* data release

R. L. Smart,[1,2★†] F. Marocco,[2★] J. A. Caballero,[3,4★] H. R. A. Jones,[2] D. Barrado,[4] J. C. Beamín,[5,6] D. J. Pinfield[2] and L. M. Sarro[7]

[1] *Istituto Nazionale di Astrofisica, Osservatorio Astrofisico di Torino, Strada Osservatorio 20, I-10025 Pino Torinese, Italy*
[2] *School of Physics, Astronomy and Mathematics, University of Hertfordshire, College Lane, Hatfield AL10 9AB, UK*
[3] *Landessternwarte Königstuhl, Zentrum für Astronomie der Universität Heidelberg, Königstuhl 17, D-69117 Heidelberg, Germany*
[4] *Centro de Astrobiología, Department Astrofisica INTA-CSIC, ESAC campus, Camino Bajo del Castillo s/n, E-28692, Villanueva de la Cañada, Madrid, Spain*
[5] *Instituto de Física y Astronomía, Universidad de Valparaíso, Ave. Gran Bretaña, 1111, Valparaíso, Chile*
[6] *Millennium Institute of Astrophysics, Santiago, Chile*
[7] *Departamento de Inteligencia Artificial, ETSI Informática, UNED, Juan del Rosal, 16 E-28040 Madrid, Spain*

Accepted 2017 March 27. Received 2017 March 27; in original form 2017 February 17

ABSTRACT

We identify and investigate known ultracool stars and brown dwarfs that are being observed or indirectly constrained by the *Gaia* mission. These objects will be the core of the *Gaia* ultracool dwarf sample composed of all dwarfs later than M7 that *Gaia* will provide direct or indirect information on. We match known L and T dwarfs to the *Gaia* first data release, the Two Micron All Sky Survey and the *Wide-field Infrared Survey Explorer* AllWISE survey and examine the *Gaia* and infrared colours, along with proper motions, to improve spectral typing, identify outliers and find mismatches. There are 321 L and T dwarfs observed directly in the *Gaia* first data release, of which 10 are later than L7. This represents 45 per cent of all the known LT dwarfs with estimated *Gaia G* magnitudes brighter than 20.3 mag. We determine proper motions for the 321 objects from *Gaia* and the Two Micron All Sky Survey positions. Combining the *Gaia* and infrared magnitudes provides useful diagnostic diagrams for the determination of L and T dwarf physical parameters. We then search the Tycho-*Gaia* astrometric solution, *Gaia* first data release subset, to find any objects with common proper motions to known L and T dwarfs and a high probability of being related. We find 15 new candidate common proper motion systems.

Key words: binaries: visual – brown dwarfs – Hertzsprung–Russell and colour–magnitude diagrams – stars: late-type – solar neighbourhood.

1 INTRODUCTION

Gaia is observing over a billion objects in our Galaxy and is revolutionizing astronomy in many areas (Gaia Collaboration et al. 2016a). One of these areas is the study of the bottom of the main sequence and beyond. L and T (hereafter LT) dwarfs are very cool faint objects that are either substellar or at the stellar–substellar boundary (Delfosse et al. 1997; Kirkpatrick et al. 1999; Martín, Basri & Zapatero Osorio 1999; Burgasser et al. 2006a; Dieterich et al. 2014). In the billion-object catalogue of *Gaia*, there will be direct observations of about a thousand LT dwarfs (Sarro et al. 2013; Smart 2014). This sample, even though it is relatively small, will be more homogeneous, accurate, complete and larger than the current catalogue of known L and early T dwarfs with measured parallactic distances.

The reason for the relative paucity of LT dwarfs in the *Gaia* observations is because they emit predominantly in the infrared and are very faint in the *Gaia* bands (see Fig. 1). However, *Gaia* will provide a magnitude-limited complete sample of the early LT spectral types in the solar neighbourhood. The nominal *Gaia G* magnitude limit is 20.7 mag and we expect the mission to be complete to $G = 20.3$ mag (Gaia Collaboration et al. 2016b). Internal validation, with models and clusters, finds a completeness of 50 per cent at $G = 20.3$ mag for the *Gaia* first data release (hereafter DR1).[1] In Table 1 we report the distance limits for L0 to T9 objects with a *G* limit of 20.3 mag and 20.7 mag using equation (2)

★E-mail: smart@oato.inaf.it (RLS); f.marocco@herts.ac.uk (FM); caballero@cab.inta-csic.es (JAC)
†Leverhulme Visiting Professor.

[1] http://gaia.esac.esa.int/documentation/GDR1/

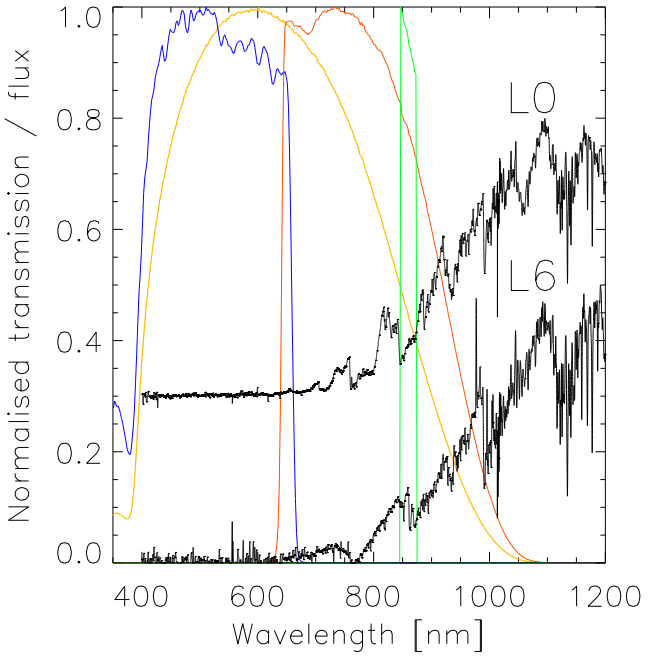

Figure 1. Normalized instrumental transmission for *Gaia G* (yellow), G_{BP} (blue), G_{RP} (red) and G_{RVS} (green) filters and optics. The spectra marked L0 and L6 are from X-Shooter for the L0 dwarf 2MASS J23440624−0733282 and the L6 dwarf 2MASS J00065794−6436542, arbitrarily scaled and off set from each other.

Table 1. Distance limits for L0 to T7 spectral types using equation (2). $D_{G<20.3}$ =distance limit assuming $G<20.3$ mag and $D_{G<20.7}$ for $G<20.7$ mag.

L SpT	$D_{G<20.3}$ (pc)	$D_{G<20.7}$ (pc)	T SpT	$D_{G<20.3}$ (pc)	$D_{G<20.7}$ (pc)
L0	69	82	T0	12	14
L1	55	67	T1	12	14
L2	45	54	T2	12	14
L3	36	44	T3	12	14
L4	29	35	T4	11	14
L5	24	29	T5	10	12
L6	19	23	T6	8	10
L7	16	19	T7	6	7
L8	13	15	T8	3	4
L9	10	12	T9	2	2

developed in Section 3.1. In addition to solar-metallicity LT dwarfs, *Gaia* will also provide a volume limited sample of old thick disc or halo L-type subdwarfs, and young LT objects in the solar neighbourhood.

Other LT and even cooler Y dwarfs (Cushing et al. 2011) will be indirectly detected in *Gaia* observations, for example, as low-mass companions in unresolved binary systems (Pope, Martinache & Tuthill 2013; Littlefair et al. 2014; Sozzetti et al. 2014; Burgasser et al. 2015; Ma et al. 2016) and as gravitational microlenses (Belokurov & Evans 2002; Proft, Demleitner & Wambsganss 2011; Ranc & Cassan 2014; Sahu et al. 2014). *Gaia* will constrain other LT and Y dwarfs in common proper motion (CPM) systems of wide binaries or moving groups where distances and kinematics of the brighter members, visible to *Gaia*, can be matched to the fainter objects with kinematics found from other surveys.

Ultracool dwarfs (UCDs) are defined as objects later than M7 (see Jones & Steele 2001). We have begun a systematic project to catalogue and characterize the cooler part of the *Gaia* Ultracool Dwarf sample (hereafter GUCDS), being all L, T and Y dwarfs that *Gaia* will directly observe or indirectly constrain. The GUCDS will be the primary sample in the near future to test atmospheric models and evolution scenarios, and to derive fundamental properties of objects at the end of the main sequence.

Here, we find the LT dwarfs directly observed by *Gaia* as isolated objects with an identifiable entry in the *Gaia* DR1 and we find those LT dwarfs in CPM systems with the *Gaia* DR1 subset with astrometric solutions. In Section 2 we describe the L, T and Y dwarf input catalogue used to search the *Gaia* DR1; in Section 3 we describe the production of the GUCDS catalogue of known matched LT dwarfs; in Section 4 we describe the discovery of new CPM candidates; in Section 5 we discuss the two catalogues in various magnitude, colour and proper motion parameter spaces and in the last section we summarize the results.

2 CATALOGUE OF KNOWN L, T AND Y DWARFS

2.1 Input catalogue

LT dwarfs seen by *Gaia* will all be nearby (d < 82 pc; Table 1) and, therefore, have significant proper motions. With this in mind, we used as the starting point for our input catalogue of known late M, L, T and Y dwarfs the online census being kept by J. Gagné.[2] This included objects from the Dwarf archives,[3] the work of Dupuy & Liu (2012), and the PhD thesis catalogue of Mace (2014). To this compilation, we added the objects in Marocco et al. (2015) and Faherty et al. (2016). We did not include the significant number of UCD candidates with photometry-based spectral types (e.g. Folkes et al. 2012; Smith et al. 2014; Skrzypek, Warren & Faherty 2016), since they are mostly too faint for *Gaia* and do not yet have proper motion estimates.

We confine our sample to all objects that have an optical or infrared spectral type equal to or later than L0 or are young late type M dwarfs that are probable brown dwarfs (e.g. TWA 27 A; Gizis 2002). These objects cover a large age range and include objects in the stellar, brown dwarf and giant-planet regimes. While *Gaia* is only observing directly a few objects later than L7, we included all published L, T and Y dwarfs, as the same list is used to search for CPM objects in the *Gaia* DR1. Most UCDs (in particular late-M and early-L dwarfs) have been classified using both their optical and near-infrared spectra, leading to two different and sometimes discordant spectral types. When we had to choose a spectral type, for example to calculate spectroscopic distances, we adopted optical spectral types for late-M and L dwarfs when available, since the wealth of spectral lines and bands in the 5000–10 000 Å wavelength range makes the classification more accurate, while for T dwarfs we use their near-infrared spectral type following similar considerations.

The current version of the input catalogue contains 1885 entries. In Table 2 we list the short name, discovery name, equatorial coordinates, adopted spectral type, proper motions and J-band magnitude of the first five UCDs of the list. The full GUCDS input catalogue with references for each variable is available online. This list will evolve, and be updated and maintained, as part of the GUCDS initiative in the MAIA data base (Caballero 2014).

[2] https://jgagneastro.wordpress.com/list-of-ultracool-dwarfs/
[3] http://www.dwarfarchives.org/

Table 2. The GUCDS input catalogue.[a]

GUCDS ID	Name	α (deg)	δ (deg)	Spectral type	$\mu_\alpha \cos\delta$ (mas yr^{-1})	μ_δ (mas yr^{-1})	J (mag)
J0000+2554	2MASS J00001354+2554180	0.056 4165	+25.905 000	T4.5[2]	+6 ± 19	+130 ± 22	15.063
J0001+1535	2MASS J00011217+1535355	0.300 7080	+15.593 194	L4[2]	+150 ± 19	− 169 ± 19	15.522
J0001−0841	2MASS J00013166−0841234	0.383 0416	−8.690 806	L1 p(blue)[2]	+331 ± 14	− 299 ± 14	15.712
J0002+2454	2MASS J00025097+2454141	0.712 3755	+24.903 917	L5.5[2]	+2 ± 23	− 36 ± 29	17.165
J0004−6410	2MASS J00040288−6410358	1.012 0000	−64.176 611	L1 γ[1]	+64 ± 5	− 47 ± 12	15.786
...	...	...	...	...	...	...	...

Notes. [a]The full table of 1886 entries is available online, references for each variable are in the online version. Superscripts[1] and [2]indicate that the adopted spectral type were measured in the optical and near-infrared, respectively.

2.2 Predicted *G* magnitude

To first estimate a *Gaia G* magnitude for the input catalogue, we used the procedure developed in Smart (2014). Briefly, we combined the Two Micron All Sky Survey (hereafter 2MASS; Skrutskie et al. 2006) *J* magnitudes, Sloan Digital Sky Survey (hereafter SDSS; York et al. 2000) colours as a function of spectral type from table 3 in Hawley et al. (2002), and colour transformations between *Gaia* photometry and the SDSS system from Jordi (2012) to find a predicted *G* magnitude. To this table we fitted a simple linear polynomial of predicted *G* magnitudes as a function of spectral type and *J* magnitude to obtain:

$$G_{\rm pred} = J - 12.63 + 0.244\ {\rm SpT}, \quad (1)$$

where SpT is the numerical representation of the LT types from 70 to 89 equivalent to L0 to T9.

The Jordi (2012) *Gaia*-to-SDSS transformations were based on main-sequence stars in the colour range $g - r = (-0.5, 7.0)$ mag. There will be a systematic error in equation (1) due to the difference between M and LT dwarf spectral energy distributions, but we estimated this to be less than 0.2 mag by extrapolating the difference between M giants and dwarfs in the transformation construction. The transformation is imprecise because of the multiple steps, the use of 2MASS magnitudes and this systematic error. However, equation (1) was only used to constrain the objects that we search for, so we considered it sufficient. From the input list we searched the *Gaia* DR1 for all objects with a predicted magnitude $G_{\rm pred} < 23$ mag. Since the nominal DR1 limit is $G = 20.7$ mag, this allowed for significant random or systematic errors in our relationship and its parameters (*J*, SpT). Of the original 1885 objects, 1317 were brighter than this conservative $G_{\rm pred} < 23$ mag cut. In the final matched catalogue the faintest object had a $G_{\rm pred} = 22.6$ mag.

3 IDENTIFICATION OF DR1 MATCHES

3.1 Initial matching

Since our input objects generally have high proper motions, and both the ground-based GUCDS input catalogue and the DR1 are of different epochs and with varying completeness, the identification of the LT dwarfs in the DR1 required a careful cross match. For each object, we matched the published position moved to the DR1 epoch using the proper motions in our input list. We found that 328 of the 1317 UCDs had a DR1 entry within a matching radius of 3 arcsec. We also considered other matching radii both smaller (2 arcsec) and larger (5 arcsec), and found 3 arcsec to be the best compromise between too many false matches and missing true high proper motion objects. Of these, six objects had more than one DR1 match within 3 arcsec, and eight had a non-zero *duplicated_source* flag in the DR1, which indicates that during the *Gaia* processing the source at some point was duplicated.

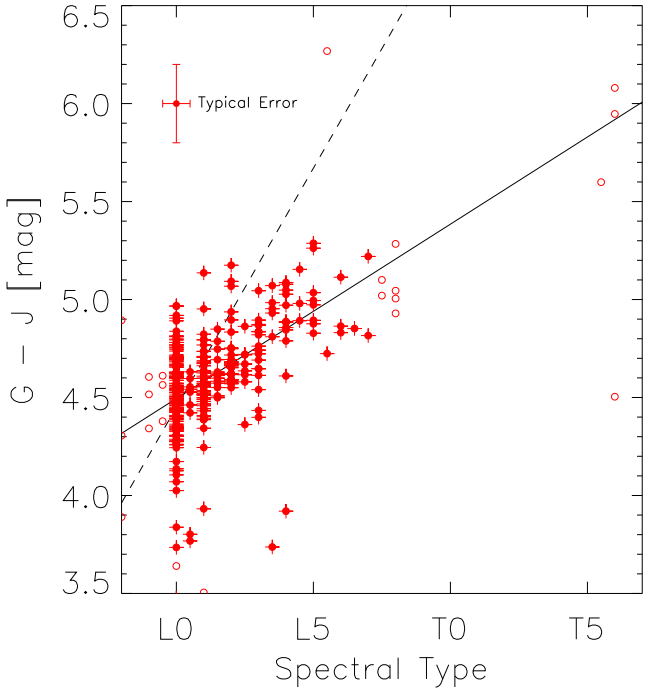

Figure 2. All matched 328 objects $G - J$ magnitude versus spectral type plotted as open circles. The 304 filled circles are L0−7 dwarfs with one matched DR1 entry within 3 arcsec and a zero DR1 *duplicated_source* flag used to find the solid line (equation 2). The dashed line is the $G_{\rm pred}$ found from equation (1). See Section 3.1 for details. Typical error bars are shown.

We then determined a new relationship for estimating *G* magnitudes from 2MASS *J* magnitudes and tabulated spectral types. We selected the 304 cross-matched L dwarfs that (*i*) had only one DR1 match within 3 arcsec, (*ii*) had a zero *Gaia duplicated_source* flag, and (*iii*) were earlier than L7. For this subsample, using least squared absolute deviation we found the first-order polynomial relationship between the colour $G - J$ and spectral type as:

$$G_{\rm est} = J - 1.098 + 0.080\ {\rm SpT} \quad (2)$$

valid for SpT = 70 to 77, i.e. L0 to L7.

The colour–spectral type diagram in Fig. 2 illustrates the measured *G* minus *J* magnitudes with lines that represent $G_{\rm pred}$ (equation 1), and this new robust fit, $G_{\rm est}$ (equation 2). The new relation in equation (2) is much flatter than equation (1). We found seven objects with a measured and estimated *G* difference, $\Delta G = |G - G_{\rm est}|$, larger than 1 mag. While the underestimation of the $G - J$ for the T6 object indicates extrapolating the fit beyond L7 provides

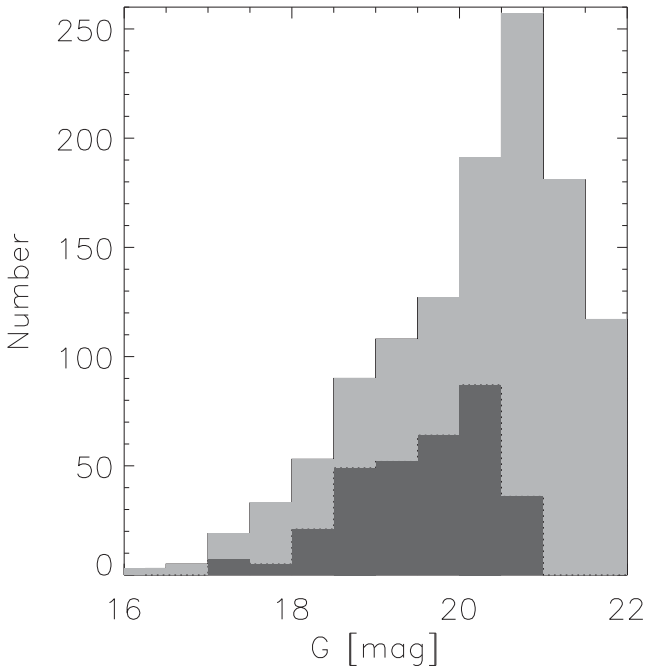

Figure 3. Distribution histograms of $G_{\rm est}$ for the input catalogue (light grey) and of *Gaia* measured G magnitudes (dark grey).

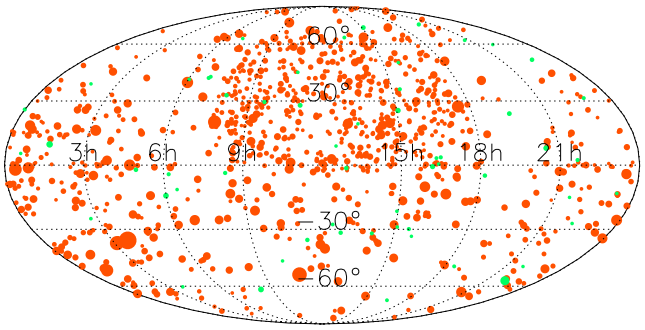

Figure 4. The equatorial distribution of 1010 L (red) and 58 T (green) dwarfs with $G_{\rm est} < 21.5$ mag. The size of the symbol indicates the $G_{\rm est}$ magnitude – larger is brighter.

uncertain results, we only used this ΔG flag as an indicator of possible problems.

Fig. 3 is the distribution of the input catalogue in $G_{\rm est}$ magnitudes using equation (2) for the input catalogue and the 328 matched objects with measured G magnitudes. The degree of completeness varies greatly from 0 per cent in the bright bins below $G = 16.5$ mag and the faint bins beyond $G = 21$ mag to over 50 per cent at $G = 19$ mag. The brightest bins have the objects with the highest proper motions and so are systematically affected by *Gaia* observation matching problems (Fabricius et al. 2016). In general, the incompleteness can be attributed to objects that were excluded from DR1, matching problems due to imprecise positions and/or proper motions or mis-classifications in the GUCDS input catalogue leading to overestimated $G_{\rm est}$ magnitudes.

In total, there are 1010 L and 58 T dwarfs brighter than $G_{\rm est} = 21.5$ mag, and 543 L and 10 T dwarfs brighter than $G = 20.3$ mag. In contrast, Smart (2014) predicted only two T dwarfs to $G = 20.3$ mag. The higher number estimated in this work is due to the systematic underestimation of the $G_{\rm pred}$ (equation 1) used in Smart (2014) with respect to the $G_{\rm est}$ (equation 2). Using a more theoretical approach, Sarro et al. (2013) predicted of the order of 10 T dwarfs brighter than $G = 20.0$ mag.

In Fig. 4, we plot the sky distribution of all the input catalogue with $G_{\rm est} < 21.5$ mag using equation (2). The region of overdensity in the Northern hemisphere is from the SDSS footprint, and is probably representative of a complete sky (Schmidt et al. 2010). However, the Galactic plane is incomplete, as most of the LT dwarfs discovered to date have been via photometric selection, and the crowding in the plane makes this difficult.

Of the six objects that had more than one DR1 entry within 3 arcsec some may be due to binarity or a background object near to the catalogue dwarf, but most are due to multiple entries in the DR1 (see section 4 in Gaia Collaboration et al. 2016b). It is estimated that the multiple entries in the DR1 catalogue are a few per cent (Fabricius et al. 2016), consistent with this finding.

In the GUCDS input catalogue, objects either have published proper motions or we estimated them from the 2MASS and *Wide-field Infrared Survey Explorer* (*WISE*) AllWISE[4] positions (Wright et al. 2010). We compared these input values with a derived proper motion from the difference of the *Gaia* DR1 and the 2MASS position. When the magnitude of the proper motions differed by more than 20 per cent, we flagged the object. This resulted in 145 objects being flagged, i.e. $\sim$ 50 per cent. This high percentage is not unexpected given that both proper motions are of low precision and the parallactic motion of the object is unknown.

3.2 Identifying mismatches

Since *Gaia* does not produce images (in general), we cannot perform the usual visual confirmation to look for mismatches. We confined our examination for mismatches to the catalogue maps and various flags. For each target we constructed a quality assurance output including: the flags for proper motion and $|G - G_{est}|$ magnitude differences; number of DR1 observations; the 2MASS images; positions and magnitudes from the 2MASS, AllWISE and DR1 catalogues; the input spectral types; parallaxes when published; input comments (e.g. known binarity or subdwarf); literature and calculated proper motions; and plots of the fitted proper motions and sky maps for the field in 2MASS, AllWISE and DR1 catalogues.

In Fig. 5 we show an example of the sky distribution plots for the field around the T6 J0817−6155 (Artigau et al. 2010). The slight misalignment between the cross and the square in the DR1 panel is due to imprecise starting proper motions from the input catalogue. When needed, we also examined online ground-based images of the fields.

We examined all 328 targets to see if any of the candidates were obvious mismatches. In particular, we paid special attention to the objects with large magnitude differences, multiple DR1 entries within 3 arcsec and the 10 objects later than L7. Of the 328 targets, we identified three objects that we believe are mismatches and are listed in Table 3. Most of these had $\Delta G > 1.0$ mag, proper motion differences larger than 20 per cent, and/or visual inspection of the field did not allow an unambiguous identification. The *Gaia* second data release is expected to resolve these ambiguities.

3.3 DR1 multiple matches

There are six LT dwarfs with multiple matches within 3 arcsec. Three, J0257−3105 (Kirkpatrick et al. 2008), J0543+6422 (Reid

[4] http://irsa.ipac.caltech.edu/data/download/wise-allwise/

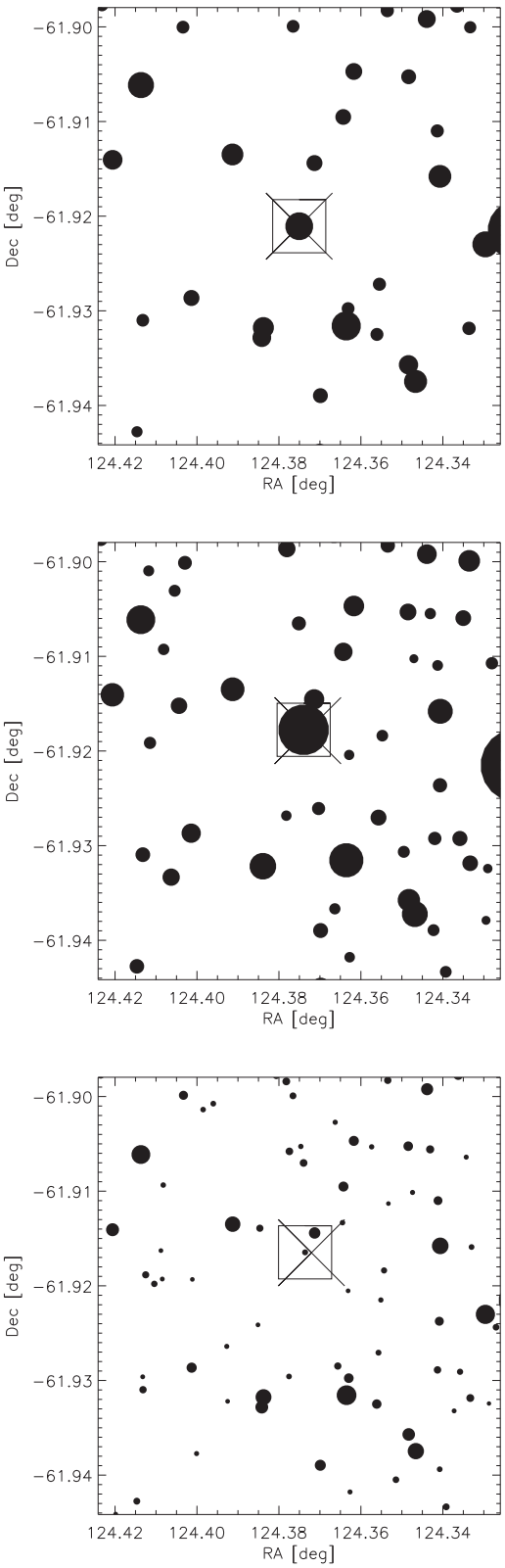

Figure 5. Sky plots of a 2.5×2.5 arcmin field around J0817−6155 in 2MASS *J* (top panel, epoch 2000.0), AllWISE *W2* (middle, epoch 2010.6) and DR1 *G* (bottom, epoch 2015.0). Brighter objects are plotted as larger symbols. The 'X' matches the predicted position based on the literature position and proper motions, the 20 arcsec^2 is centred on the respective catalogue source.

et al. 2008) and J1515+4847 (Wilson et al. 2003), are matched to DR1 entries within only 1 arcsec and the DR1 entries have very similar magnitudes. The matches to these three are probably duplicated DR1 entries (see discussion in Fabricius et al. 2016), and we adopted the DR1 entry with the highest number of observations. The candidate J1203+0015 (Fan et al. 2000) is matched to two entries with significantly different magnitudes (both fainter than the estimated *Gaia* magnitude) so either it is probably close to a background object or *Gaia* has resolved the dwarf into a binary system with a 0.3 arcsec separation. The targets J1606−2219 and J1607−2211 (Lodieu et al. 2007) have fainter detections 2–3 arcsec away, which we believe to be background objects. In these last three cases we adopted the match closest to the predicted LT dwarf position.

3.4 Completeness

If we consider input catalogue objects with $G_{\rm est} < 20.3$ mag we find only 45 per cent in the *Gaia* DR1. This incompleteness is primarily due to the quality assurance cuts of *Gaia* which are $N > 5$, $\epsilon_i < 20$ mas and $\sigma_{\rm pos,\,max} < 100$ mas, where N is the number of field-of-view transits used in the solution, ϵ_i is the excess source noise and $\sigma_{\rm pos,\,max}$ is the semimajor axis of the error ellipse in position at the reference epoch (from section 5 in Lindegren et al. 2016). In addition, we required all included objects to have valid photometry. The number of field-of-view transits led to a systematic incompleteness that follows the scanning law and can be seen in the sky plots of *Gaia* DR1.[5] Importantly for these objects, the cyclic processing does not yet use internal proper motions to update the position of objects during the matching, so the correct matching of high proper motion objects is deficient (Fabricius et al. 2016). Given the documented incompleteness of 50 per cent at $G = 20.3$[6] mag, and the very high proper motion of most bright LT dwarfs, we consider the success rate of 45 per cent to be reasonable. The matching for DR2 will include internal proper motions, so it will not have this deficiency.

3.5 *Gaia* observed L and T dwarf catalogue

We produced a catalogue of the parameters for the 321 L and T dwarfs with a reliable entry in *Gaia* DR1, which are distributed as shown in Fig. 6. This will be actively updated online along with the input catalogue. In Table 4 we report new parameters for the first five objects from this catalogue table with: DR1 positions; calculated proper motions with errors; G magnitudes and errors; number of observations in DR1; *Gaia* Source ID; $\Delta G = G - G_{\rm est}$; number of DR1 entries within 3 arcsec and a flag that indicates if the calculated proper motion was within 20 per cent of the published or estimated value. The published catalogue also has other literature information such as 2MASS and *WISE* magnitudes for each entry.

4 COMMON PROPER MOTION LT DWARFS AND DR1 STARS

4.1 The Tycho-*Gaia* astrometric subset

The *Gaia* DR1 included a subset of more than 2 million objects that incorporated earlier positional information to find parallaxes

[5] http://sci.esa.int/gaia/58209-gaia-s-first-sky-map
[6] http://gaia.esac.esa.int/documentation/GDR1/

Table 3. Input catalogue objects with mismatches in *Gaia* DR1.

Name	*Gaia* DR1 Source ID	ΔG[mag]	Remarks
WISEPA J062720.07−111428.8[1]	3000505938722626560	− 1.4	Probable satellite of galaxy USNO-B1 0787−0079432
USco J160714.79−232101.2[2]	6242316978518793856	− 1.4	Star or galaxy USNO−B1 0666−0359684
USco J163919.15−253409.9[3]	6046485475060342528	− 1.1	Star or galaxy USNO−B1 0644−0382256
WISE J170745.85−174452.5[4]	4135505777467362304	− 2.6	In crowded region towards Galactic Centre
2MASS 18000116−1559235[5]	4145132555890843520	1.3	In crowded region of low Galactic latitude
WISE J200403.17−263751.7[6]	6850032688873127424	− 0.9	Star or galaxy USNO−B1 0633−0938809
WISE J223617.59+510551.9[4]	1988335902592180608	− 0.3	Star or galaxy USNO−B1 1410−0455016

Discovery references: [1]Kirkpatrick et al. (2011), [2]Lodieu et al. (2007), [3]Lodieu et al. (2009), [4]Mace et al. (2013), [5]Folkes et al. (2012), [6]Thompson et al. (2013).

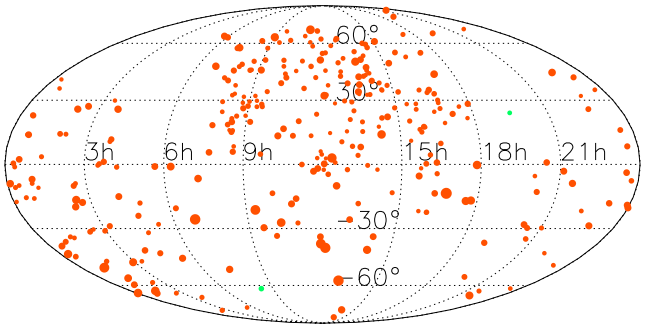

Figure 6. Same as Fig. 4, but for the 321 L (red) and T (green) dwarfs with an entry in *Gaia* DR1.

and proper motions called the Tycho-*Gaia* astrometric solution (TGAS; Michalik, Lindegren & Hobbs 2015; Gaia Collaboration et al. 2016b). We selected CPM pairs by cross-matching our catalogue of known LT dwarfs with the TGAS subset. For the input LT dwarfs we used measured parallaxes from the literature, complemented with spectrophotometric distances estimated using the adopted UCD spectral types and near-infrared magnitudes. To estimate their spectrophotometric distance we used the polynomial relations presented in Dupuy & Liu (2012), with the measured 2MASS J magnitude, and, if not available or the 2MASS value has a bad quality flag (Qflag = U), we use the MKO J magnitude.

4.2 Selection criteria

The starting CPM candidate list was generated from finding all TGAS stars within 2° of our input LT dwarfs and applying the following criteria:

(i) $\mu > 100$ mas yr^{-1}
(ii) $\Delta\mu_\alpha \cos\delta < 20$ mas yr^{-1} and $\Delta\mu_\delta < 20$ mas yr^{-1},

where μ is the total proper motion, $\Delta\mu_\alpha \cos\delta$, $\Delta\mu_\delta$ are the difference between the proper motion components of the UCD and the TGAS star. All selected TGAS objects are close so we do not need to invoke inference techniques to find distances (e.g. Bailer-Jones 2015), but use the simple inverse of the parallax as the estimated distance and as its error, a proportion equal to the relative error of the parallax. We then calculated a chance alignment probability for each system following the method described in Marocco et al. (2017).

The selection criteria require the objects to have relatively high proper motions and the probability of having two objects with such high proper motions in a limited area is already small. For each candidate pair we used the sample of all TGAS field stars in a radius of 2° from the UCD to determine the distance and proper motion distribution of the field population. The distance and proper motion distribution were treated as a probability density function, which we reconstructed using a kernel density estimation. We then drew 10 000 samples of stars from the reconstructed probability density function and determined how many 'mimics' of our system were generated. We considered any star within 3σ of the distance and proper motion of our selected primaries as a mimic of our CPM system. The chance alignment probability was assumed to be the number of mimics divided by 10 000. If this probability was below 6×10^{-5}, equivalent to a 4σ level, we consider the pair to be a 'robust' CPM system. Systems with larger chance alignment probability were ruled out.

4.3 LT dwarfs and *Gaia* CPM system catalogue

This selection yielded a sample of 32 CPM pair candidates. We compiled a list of known binary and CPM systems by combining the objects and list from the following publications: Mason et al. (2001), Deacon et al. (2014, 2017), De Rosa et al. (2014), Dhital et al. (2015), Gauza et al. (2015), Smith et al. (2015), Scholz (2016),

Table 4. New parameters for the GUCDS-DR1 catalogue.[a]

Short name	*Gaia* source ID	α, δ (deg)	$\mu_\alpha\cos\delta$, μ_δ (mas yr^{-1})	G (mag)	ΔG (mag)	$N_{\rm obs}$, N_3, F_μ
J0006−1720	2414607592787544320	1.585253567, −17.347415311	−41 ± 11, 0 ± 12	20.525 ± 0.043	0.163	97,0,1
J0006−0852	2429054454021227648	1.704590901, −8.880825977	−61 ± 12, −324 ± 12	18.485 ± 0.008	−0.078	239,0,0
J0006−6436	4900323420040865792	1.742217614, −64.615322431	82 ± 5, −65 ± 13	17.988 ± 0.011	0.103	145,0,0
J0016−1039	2428008410441149824	4.156258155, −10.653818836	−111 ± 12, −193 ± 12	20.028 ± 0.022	0.073	185,0,0
J0018−6356	4900453540369793408	4.695160455, −63.938248147	324 ± 6, −381 ± 13	19.774 ± 0.025	−0.110	108,0,0
...	...	...	...	...	...	...

Notes. [a]Equatorial coordinates and apparent magnitudes are from *Gaia* DR1 at epoch J2015.0, while proper motions were computed by us after using 2MASS and *Gaia* astrometry. $\Delta G = G - G_{\rm est}$; $N_{\rm obs}$ = number of *Gaia* observations; N_3 = number of DR1 entries within 3 arcsec and F_μ is a flag to indicate if the calculated proper motion was within 20 per cent of the input value. The full table of 321 LT dwarfs with other supporting magnitudes is references are available online.

Table 5. The common-distance, CPM pair candidates identified here. A machine readable version of this table is available online.

Name	α (deg)	δ (deg)	$\mu_\alpha \cos\delta$ (mas yr^{-1})	μ_δ (mas yr^{-1})	d (pc)	PDF	Proj. Sep. (10^3 au)	SpT
HIP 10346	33.317 68 733	− 59.567 00 153	126.5 ± 0.1	− 8.3 ± 0.1	58.4 ± 1.8	2.2e-05	400	
J0223−5815	35.977 66 900	− 58.251 87 300	134.0 ± 10.0	5.0 ± 19.0	49.0 ± 10.0			
HIP 12158	39.175 35 990	− 3.155 89 420	323.4 ± 0.1	58.2 ± 0.1	24.1 ± 0.2	3.6e-08	145	
J0230−0225	37.662 14 300	− 2.431 67 270	329.0 ± 16.8	51.3 ± 14.9	27.0 ± 6.0			
TYC 146-1101-1	97.547 55 003	0.876 48 584	68.4 ± 2.9	− 105.7 ± 2.4	67.6 ± 1.0	3.3e-06	252	
J0626+0029	96.588 39 400	0.492 81 806	84.0 ± 15.0	− 92.0 ± 15.0	67.0 ± 14.0			
HIP 38492	118.247 96 721	22.556 12 499	− 85.9 ± 0.2	− 61.4 ± 0.1	34.2 ± 0.3	3.0e-07	157	
J0758+2225	119.624 29 000	22.424 08 300	− 105.0 ± 8.0	− 62.8 ± 8.2	33.0 ± 8.0			
TYC 230-109-1	139.992 73 886	4.999 44 728	− 80.0 ± 1.2	− 40.2 ± 1.1	42.2 ± 0.7	1.5e-07	178	
J0915+0531	138.933 88 000	5.517 80 560	− 95.0 ± 5.5	− 57.7 ± 4.4	33.0 ± 6.0			
TYC 2504-466-1	145.552 16 670	33.929 92 123	− 103.7 ± 3.8	− 67.3 ± 1.6	61.5 ± 1.9	1.1e-06	156	
J0939+3412	144.777 13 000	34.215 96 100	− 107.1 ± 10.4	− 64.3 ± 12.6	62.0 ± 12.0			
HIP 47704	145.897 19 170	10.518 34 984	37.5 ± 0.1	− 124.9 ± 0.1	71.7 ± 1.2	2.5e-06	211	
J0943+0942	145.956 67 000	9.700 94 440	45.4 ± 10.9	− 119.9 ± 8.8	79.0 ± 15.0			
TYC 824−423-1	145.449 63 031	11.175 17 624	64.6 ± 0.9	− 111.1 ± 0.7	102.8 ± 3.2	8.2e-06	576	
J0943+0942	145.956 67 000	9.700 94 440	45.4 ± 10.9	− 119.9 ± 8.8	79.0 ± 15.0			
HIP 57734	177.586 99 124	10.067 23 706	− 89.9 ± 0.1	− 16.5 ± 0.0	86.2 ± 2.2	1.2e-06	77	
J1150+0949	177.661 63 000	9.828 58 330	− 107.6 ± 17.1	− 31.9 ± 4.5	60.0 ± 27.0			
HIP 58241	179.181 53 043	− 32.267 44 260	− 178.8 ± 0.6	− 7.1 ± 0.3	35.4 ± 0.3	5.7e-06	229	
J1154−3400	178.675 96 000	− 34.010 84 900	− 161.0 ± 13.0	4.0 ± 15.0	30.0 ± 6.0			
HIP 58240	179.175 44 959	− 32.268 19 149	− 172.0 ± 0.4	− 8.3 ± 0.3	35.8 ± 0.4	4.0e-06	231	
J1154−3400	178.675 96 000	− 34.010 84 900	− 161.0 ± 13.0	4.0 ± 15.0	30.0 ± 6.0			
HIP 59887	184.228 18 632	37.484 07 627	− 107.9 ± 0.1	− 2.0 ± 0.1	87.8 ± 1.7	9.0e-06	153	
J1214+3721	183.640 24 000	37.353 27 100	− 122.6 ± 10.6	15.7 ± 13.4	82.0 ± 17.0			
HIP 62350	191.641 95 696	11.378 49 569	− 112.4 ± 0.1	− 0.5 ± 0.0	61.5 ± 1.9	1.1e-05	286	
J1244+1232	191.054 29 000	12.533 63 900	− 104.8 ± 8.6	4.5 ± 7.3	46.0 ± 8.0			
TYC 2587-1547-1	248.219 28 595	35.075 10 874	88.0 ± 0.5	− 61.8 ± 0.5	34.6 ± 0.3	1.4e-10	2	
J1632+3505	248.233 75 000	35.085 45 700	91.6 ± 9.7	− 65.3 ± 11.9	37.0 ± 8.0			
HIP 101880	309.679 56 167	− 43.732 89 384	235.1 ± 0.2	− 371.5 ± 0.1	51.4 ± 0.6	2.1e-10	270	
J2037−4216	309.463 79 000	− 42.279 22 200	229.0 ± 10.0	− 391.0 ± 10.0	51.0 ± 10.0			

Kirkpatrick et al. (2016) and Gálvez-Ortiz et al. (2017). Of the 32 CPM pair candidates 17 were previously known and the remaining 15, listed in Table 5, are presented here for the first time. The majority of new wide systems presented here are not physically bound pairs, but the low chance alignment probabilities we interpret as an indication of common origin. Intrinsically wide binaries and multiple systems can in fact become unbound due to Galactic tides and close encounters (e.g. Veras 2016; Elliott & Bayo 2016), and their ejecta would represent a new, as yet unexplored pool of benchmark systems (Pinfield et al. 2006; Yip et al. 2016). In Figs 7 and 8, we plot celestial and proper motion distributions of example unbound (J0230−0225) and bound (J1632+3505) CPM pairs discussed later.

One key element in our selection process is the requirement of common distance between the main sequence TGAS star and its potential companion. We show in Fig. 9 a comparison between the measured astrometric distance to the primaries in our CPM pairs, against the distance (astrometric or spectrophotometric) to their potential companions. Common-distance systems are highlighted in black. Uncertainties on the spectrophotometric distance dominate, and at a larger distance this results in a much larger scatter around the one-to-one correspondence line. Pairs that passed our angular separation constraint, but were rejected by the common-distance cut, consist of a foreground UCD matched to a background star. In Fig. 10 we plot only those systems that we select as having common distance, with those UCDs with measured parallaxes highlighted in green. As expected, systems with astrometric measurements are much closer to the one-to-one correspondence line than those with spectrophotometric distance estimates only. The UCD spectroscopic distances tend to be underestimated compared to the TGAS parallactic distances, e.g. the UCD is brighter than the spectral type indicates. This is as expected from unresolved binarity or a Malmquist bias-like effect as our input sample is probably biased to the brighter examples of a given spectral class bin.

4.4 Selected CPM systems

Extrapolating the simulations in Marocco et al. (2017) we predicted that the number of confirmable LT binary systems for the TGAS subset of *Gaia* DR1 is more than 100, while the number of unbound, but still CPM systems, is significantly higher. The procedures modelled in Marocco et al. (2017) did not include moving groups and disintegrating clusters as our knowledge of these systems is still in its infancy, hence the total number of CPM systems between LT dwarfs and the DR1 TGAS subset is probably many hundreds. The ongoing large-scale infrared surveys will provide a complete list of nearby LTs and at that point a comparison to *Gaia* results will also allow us to constrain many of the uncertain factors used in the Marocco et al. (2017) work.

For the illustration of the diverse characteristics and possible uses of the CPM systems presented here it is useful to consider a few of the systems individually:

(i) J0230−0225 is an L8 with a peculiar spectrum (Thompson et al. 2013) that we have associated with HIP 12158 (FT Cet), a

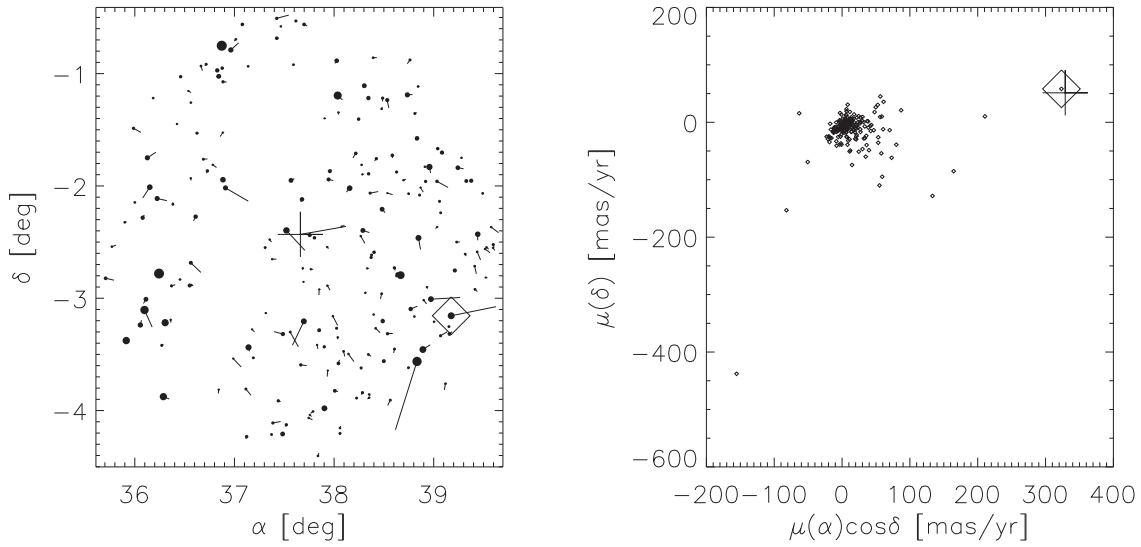

Figure 7. A probable wide CPM: TGAS objects within 2° of the L8 J0230−0225. In the left panel we show the TGAS on-sky positions with proper motions indicated by the vectors and the size of the symbols indicating the magnitude. The large diamond encloses the TGAS candidate CPM HIP 12158 and the plus sign indicates the position of J0230−0225. In the right panel we show a vector point diagram for all objects again with the cross indicating J0230−0225, the small symbols are the proper motions of the TGAS objects and the large diamond encloses HIP 12158.

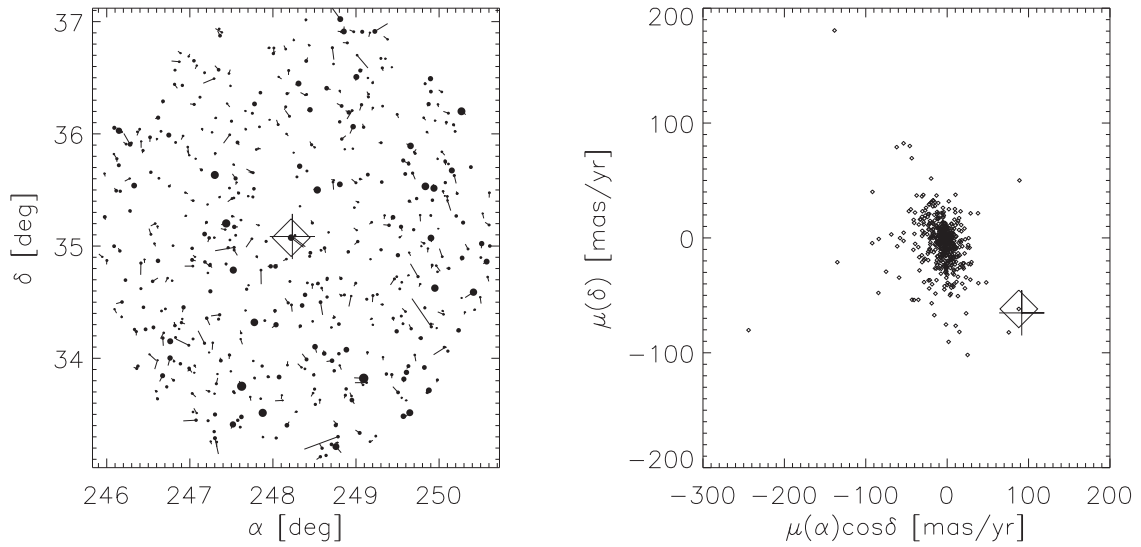

Figure 8. A probable binary: TGAS objects within 2° of the L0.5 J1632+3505. The meaning of the symbols is as in Fig. 7; however, the TGAS object, TYC 2587-1547-1, overlaps the L dwarf position in this example.

K1V star that has been indicated as a member of the Hyades Moving Group (Tabernero, Montes & González Hernández 2012). If coeval with the Hyades it will have an age between 0.4 and 1.0 Gyr and any interpretation of the spectral peculiarities will have to take that into consideration.

(ii) J0915+0531 is a T7 associated with TYC 230–109–1 (HD 80462), the primary of a visual binary system of two mid-G-type stars separated by 10 arcsec and discovered by F. G. W. Struve in the early 19th century (Mason et al. 2001). For such a binary system *Gaia* will produce precise astrometry and high-resolution RVS spectra that will provide a significant improvement on their astrophysical parameters which in turn can be used to constrain the UCD if the companionship is confirmed.

(iii) J1154−3400 (West et al. 2008) is an L0 and was proposed as a candidate member of the Argus Association (Gagné et al. 2015), which is a young 30-50 Myr system, so if this UCD is a member it is in an age regime where the radius is rapidly changing (Baraffe et al. 2002). Further work in Faherty et al. (2016) evidence that it is a very difficult case with moderate to high probabilities of being in various kinematic groups. We associate this dwarf to the primary HIP 58240 (HD 103742), in a G4V+G3V binary system with HIP 58241 (HD 103743). Adopting the precise TGAS astrometry of the binary system, it did not register as a candidate member of any moving group in either the BANYAN II (Gagné et al. 2014) or LACEwING (Riedel et al. 2017) tools to estimate probabilities of candidate objects to nearby kinematic groups. BANYAN II did

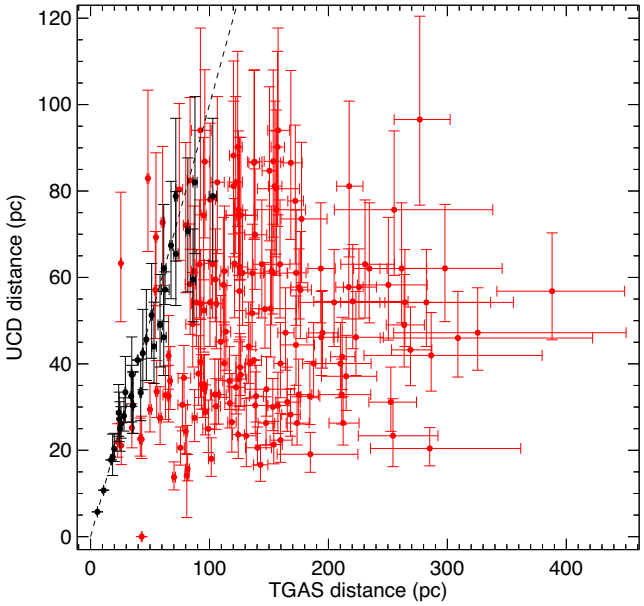

Figure 9. A comparison between the measured TGAS distance of the primaries versus distances to their candidate UCD companions for the full sample passing our angular separation and proper motion selection. Systems selected as common distance are plotted in black, while those rejected are plotted in red.

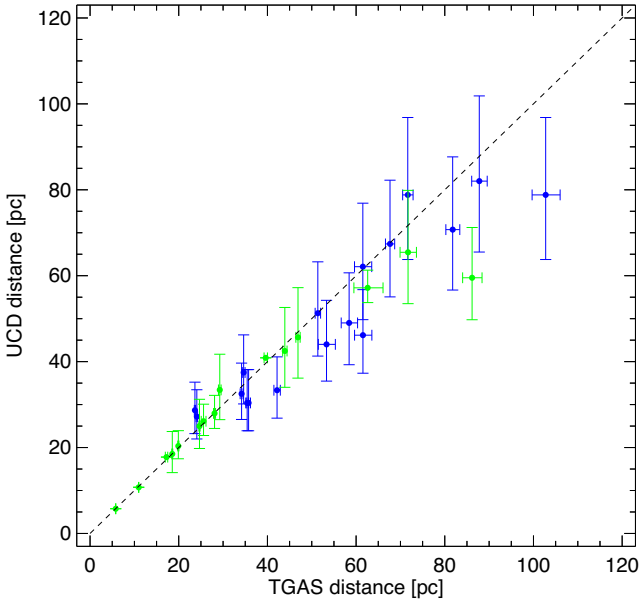

Figure 10. A comparison of TGAS and UCD distances for common-distance selected systems. Systems where the UCD has a measured parallax are plotted in green, while those with only spectrophotometric distance estimates are plotted in blue.

indicate the system maybe young (probability of being a young field object is 47 per cent against old field object of 53 per cent).

Adopting our proper motion of J1154−3400 and its parallax from Faherty et al. (2009) in BANYAN II we find there is an indication that it may be a member of Argus (probability 53 per cent) or the TW Hydrae Association (probability 10 per cent) while LACEwING gives zero probabilities for all moving groups. If the connection to the HIP 58240/58241 system is confirmed it would be hard for us to also conclude it is part of the nearby moving groups. We await future releases of the *Gaia* results to resolve these conflicting indications.

(iv) J1632+3505 (L0.5) and TYC 2587–1547–1 (HD 149361, K0 V) are separated by $\rho = 57$ arcsec at position angle $\theta = 49°$. At a heliocentric distance of 34.6 ± 0.3 pc this translates into a projected physical separation of only 1960 au and a gravitational potential energy of the order of -10^{-35} J, between 40 and 300 times larger in absolute value than the most fragile bound systems known (Caballero 2009). The relatively short projected physical separation, large absolute potential energy and similarity of recalculated proper motions of both primary and secondary with *Gaia* led us to classify this pair as the only bound system in our sample. The primary star is at the brighter end of the *Gaia* magnitude range (G=7.97 mag) while J1632+3505 is at the faint end (G=19.18 mag), so the consistency of the two *Gaia* distances will be testing both noise- and photon-limited astrometric results. The *Gaia* spectroscopic observations of the primary will lead to astrophysical parameters that can be used to constrain those of the secondary.

(v) J0943+0942 is a T4.5 that is found to be a CPM companion candidate of two TGAS stars (HIP 47704 and TYC 824-423-1). However, from the more precise proper motions of the two stars they would not be considered CPM companions. This highlights a weakness of our procedure; we calculate a probability but there will be false positives. This is one of the faintest objects that we found CPM pairs for and like most UCDs in these systems *Gaia* will not detect them; however, we expect future infrared and deep optical surveys to allow us to improve the proper motion of all UCDs.

5 AN EXAMINATION OF GUCDS MAGNITUDE, COLOUR AND PROPER MOTION RELATIONS

The *Gaia G* is a new passband from 330 to 1050 nm with transmission peaking around 600 nm and dropping to 10 per cent at 970 nm.[7]. The G magnitude represents a new resource in terms of both homogeneity and wavelength coverage, albeit with possibly limited diagnostic ability for short baseline colours due to its very wide spectral passband. It will help to constrain the spectral energy distribution of LT dwarfs across the whole of the sky in the optical. As well as this G magnitude, the second *Gaia* data release will provide both a blue and a red magnitude (G_{BP} and G_{RP}; see Fig. 1), the application of which to UCDs has been discussed at length in Sarro et al. (2013). In this section we examine the locus of UCD objects in relations among magnitude, colour and proper motion with a focus on those related to the *Gaia G* band.

5.1 Colour–colour relations

In the optical wavebands, LT dwarfs only have homogeneous magnitude estimates for parts of the sky (e.g. see Epchtein et al. 1999; Ahn et al. 2014), while in the infrared most have homogeneous magnitudes from the 2MASS and AllWISE surveys. This is also where these objects are the brightest, and combined with G produce a very long colour baseline, so here we examine the *Gaia* and 2MASS/*WISE* infrared relations. The 2MASS is 99 per cent complete to $J = 15.8$ mag[8] and, from Fig. 2, the nominal $G - J$ offset of an L0 is 4.5 mag; we therefore expect 2MASS to be complete for all *Gaia* objects with spectral types L0 and later (as they are redder) to $G = 20.3$ mag. The magnitude limit of AllWISE is $W2 = 15.7$ mag

[7] http://www.cosmos.esa.int/web/gaia/science-performance
[8] http://www.ipac.caltech.edu/2mass/overview/about2mass.html

and the colour offset is greater, so all *Gaia* LT dwarfs are expected to have an ALLWISE *W*2 detection.

In Fig. 11 we plot $J - W2$ as a function of $G - J$ and zoomed in on the LT portion of the $W2 - W3$ versus $G - W2$ graph. In Appendix A we plot the LT region in a series of combinations of *G* with 2MASS and AllWISE magnitudes. The *G*-related blue colour is always on the *X*-axis and the redder magnitude combination on the *Y*-axis. We did not include *W*4 as it is generally not sensitive enough to detect these objects. To highlight particular populations, we have plotted different symbols for the young or subdwarfs from the comments of Table 1, and the 10 objects with spectral types later than L7.

We find that the seven objects listed in Table 6, which are not indicated as young or subdwarf objects, are outliers in most colour–colour plots, and we have labelled them as 1 through 7, respectively, in the figures. If these seven objects are classed as M/L boundary dwarfs they would no longer be considered outliers as their position is with the majority of M dwarfs that dominate the background objects.

From Fig. 11 and the colour–colour plots in Appendix A we note the *Gaia*–2MASS colours differentiate the full sample better than the background sources, while the subdwarf, young objects and late LT objects are differentiated better when the AllWISE bands are used. This variation in properties makes it possible to photometrically isolate both the general LT dwarfs and also the differing subpopulations.

5.2 Spectral type and colour relations

Using the 321 candidates with DR1 photometry, we can recalibrate the $G - J$ as a function of SpT relation, which was used earlier to provide an estimated *G* value from spectral type and *J* magnitude. In Table 7 we report the mean colours, standard deviation and number of entries for all spectral bins with more than three objects.

In Fig. 12 we plot the $G - J$ and $G - W2$ with spectral type graphs, and in Appendix A we plot all of the *G*-based colours with spectral types. In addition to estimating magnitudes, these relations are useful for the identification of outlier objects, as they are reasonably monotonic for the early-L dwarfs. The onset of *Ks*-band suppression due to the atomic and molecular absorption, methane in particular (Oppenheimer et al. 1998; Noll et al. 2000; Cushing, Rayner & Vacca 2005), and collision induced absorption (Burrows et al. 2001; Kirkpatrick 2005), can be seen by the position of the two T6 objects compared to the main bulk of the targets in the $G - J$ and $G - K$ graphs. Young objects tend also to be redder in the AllWISE colours, perhaps due to circum(sub)stellar discs or enhanced dust formation due to low gravity (e.g. Zapatero Osorio et al. 2010).

5.3 Reduced proper motion diagrams

The reduced proper motion in the *G* magnitude is defined as

$$H_G = G + 5 + 5 \log \mu, \tag{3}$$

where μ is the total proper motion (Jones 1972). The H_G is correlated with the absolute magnitude in *G* via the tangential velocity. Since objects in the solar neighbourhood tend to share the same rotational velocity around the Galactic Centre as the Sun, their kinematics are restricted to velocity ellipsoids. Also since spectral types are also correlated to absolute magnitudes, a plot of H_G versus a surrogate of spectral type provides a reduced proper motion diagram, which is a powerful tool for isolating different stellar populations

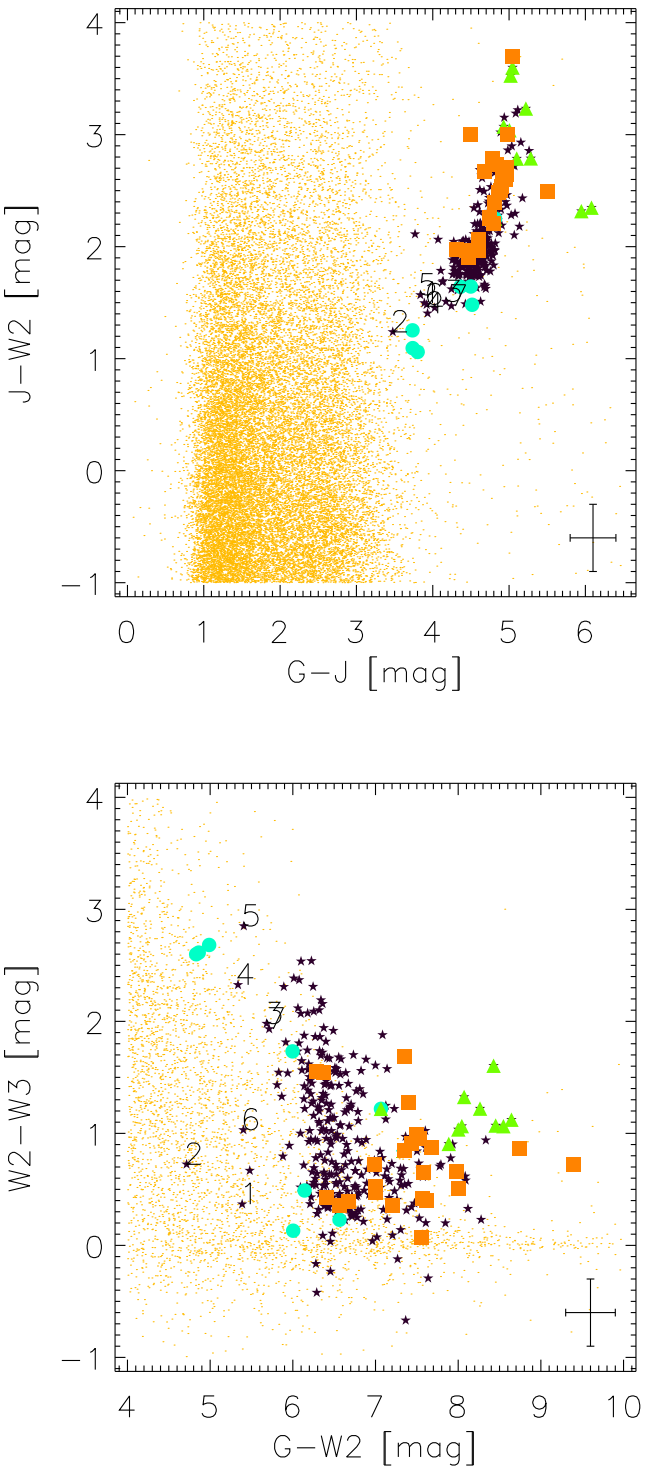

Figure 11. Colour–colour diagrams for $J - W2$ versus $G - J$ and a zoom on the LT region of the $W2 - W3$ versus $G - W2$. Filled circles are subdwarfs, squares are young dwarfs, triangles are objects later than L7, stars are other L0–6 dwarfs, and yellow points are anonymous sources within 2 arcmin of each LT dwarf. Typical error bars are shown. The seven outliers J0109−4954, J0133−6314, J1116+6037, J1245+4902, J1250+4418, J1251+6243 and J1333+1509 are labelled 1 through 7, respectively. Additional colour–colour diagrams are found in Appendix A.

Table 6. Probable late M dwarfs identified in the colour–colour and colour–spectral type diagrams.

Long name Short name Plot label	Opt SpT NIR SpT ΔG	Remarks
SSSPM J0109−4955 J0109−4954 1	M8[1] L1[2] −0.45	This object is bluer in all diagrams than we would expect for an M8 but further spectral observations are needed to clarify its spectral type.
SSSPM J0134−6315 J0133−6314 2	... L0[2] −1.02	This is the bluest LT dwarf in the majority of colour–colour plots. It has been classified as early as an M5 (Lodieu et al. 2005a) and X-Shooter spectra is a best fit with an M6 template. The *W*3 magnitude is an upper limit which explains its outlier position in the *W*3 colour combinations.
2MASS 11164800+6037309 J1116+6037 3	L0[3] ... −0.33	This is at the border of the majority of L0 colour loci. Using the best-fitting template procedure from Marocco et al. (2015) on its published SDSS spectra we find it is a late M dwarf.
2MASS 12455566+4902105 J1245+4902 4 1	L1[3] M8[4] 0.65	This object has been classified as M8[4] in the infrared and both L1[3] and M9 – (West et al. 2011) in the optical – both from SDSS spectra. It is a borderline M/L object.
2MASS 12504567+4418551 J1250+4418 5	L0[5] ... −0.66	Very blue in many colour–colour plots and comparisons of the SDSS spectra using the procedure from Marocco et al. (2015), the same spectra as used by West et al. (2008) to find L0, we find the object to be a late M dwarf. The *W*3 magnitude is an upper limit and its extreme position in the W3 colour combinations indicates that it is significantly fainter than the published value.
2MASS 12512841+6243108 J1251+6243 6	M8V[5] L4[4] −0.90	This object was listed as an L4[4] but erroneously cited as coming from Zhang et al. (2009); West et al. (2008) classified it as an M8V. Our *G* magnitude would be more consistent with the earlier type and we think this is a case of object mis-identification and the actual object is an M8V.
2MASS 13331284+1509569 J1333+1509 7	L0[3] M8[4] −0.26	This object has been classified as M8[4] in the infrared and both L0[3] and M9 (West et al. 2011) from the same SDSS spectra in the optical. It is a borderline M/L object. The *W*3 magnitude is an upper limit and it is an outlier in the ALLWISE *W*3 colour combinations so it is probably fainter.

Spectral type references: [1]Reid et al. (2008), [2]Lodieu et al. (2005b), [3]Schmidt et al. (2010), [4]Bardalez Gagliuffi et al. (2014), [5]West et al. (2008)

Table 7. Mean colours and standard deviation for all spectral type bins from L0 to L5 where there were at least three entries.

Optical SpT	$<G-J>$ (mag)	N
L0	4.52 ± 0.19	126
L0.5	4.53 ± 0.07	7
L1	4.58 ± 0.13	55
L1.5	4.63 ± 0.10	14
L2	4.70 ± 0.15	29
L2.5	4.65 ± 0.14	8
L3	4.72 ± 0.17	17
L3.5	4.95 ± 0.09	5
L4	4.92 ± 0.14	11
L4.5	5.01 ± 0.13	3
L5	5.02 ± 0.17	8

(e.g. Faherty et al. 2009; Lépine & Gaidos 2011; Jiménez-Esteban et al. 2012).

In Fig. 13, we plot the reduced proper motion H_G versus $G-J$ and $G-W3$ for the LT dwarfs identified in the DR1, and include anonymous objects within 2 arcmin of each LT dwarf with proper motions calculated in the same way (i.e. *Gaia* DR1–2MASS). The plots with other *G* and 2MASS and AllWISE colours are included in Appendix A. The anonymous objects trace out the locus of the combined thin and thick discs, while the majority of LT dwarfs clump in a relatively unoccupied region. The subdwarfs tend to occupy the lower part of the LT cloud while the young objects are on the right-hand edge.

There are 12 high proper motion objects with $H_G > 24.0$ mag listed in Table 8; these include subdwarfs and objects later than L6. For the early-L normal dwarfs, a high H_G would be an indication of a subdwarf nature; however, as H_G is a compound variable including both intrinsic magnitude and kinematical properties, it may be that it has a high velocity because of encounters that have led to an unusually high value for H_G. The distance and other parameters from *Gaia* DR2 will clarify the nature of these objects.

5.4 Hertzsprung–Russell diagrams

For the 49 targets that have published parallaxes, we can determine absolute magnitudes and tangential velocities. In Figs 14 and 15 we plot the HR diagrams with absolute *G* magnitudes and both the $G-J$ colour and the spectral type as surrogates for temperature. We have colour coded the symbols to indicate the tangential velocities. There is a spread of 0.7 mag in absolute magnitude that, based on the propagation of the formal errors, appears to be largely intrinsic. On each HR diagram we have included the most recent PHOENIX isochrones[9] (Allard, Homeier & Freytag 2013, and references therein) for a 0.005, 1 and 10 Gyr, as shown in the legends.

The objects labelled 1, 2, 3 are 2MASS 12563716−0224522, TWA 27 A and Kelu-1 A. 2MASS 12563716−0224522 is a

[9] https://phoenix.ens-lyon.fr/Grids/BT-Settl/CIFIST2011_2015/

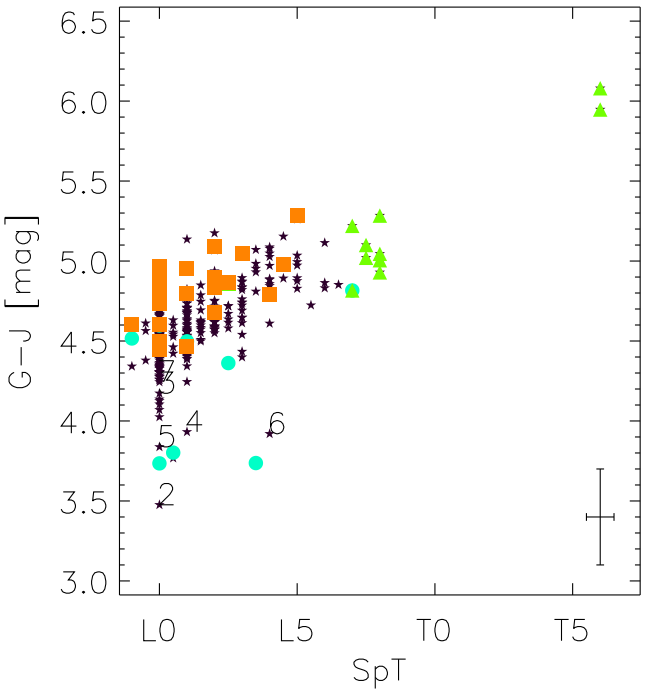

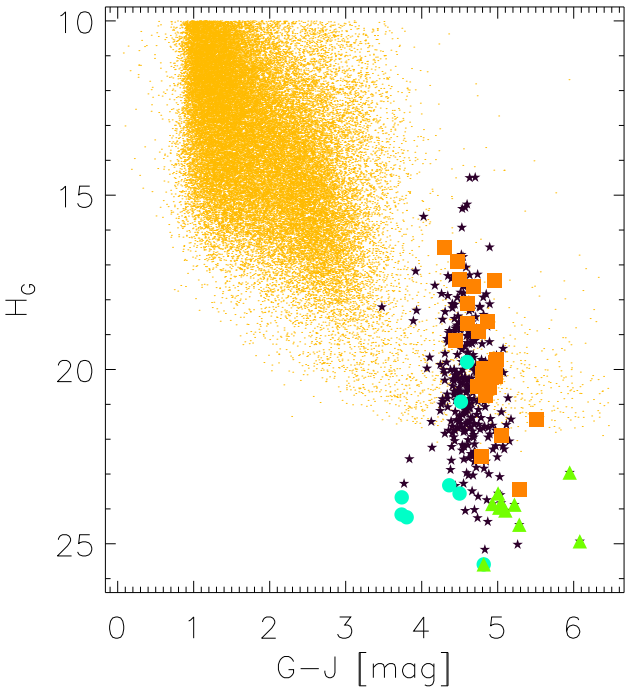

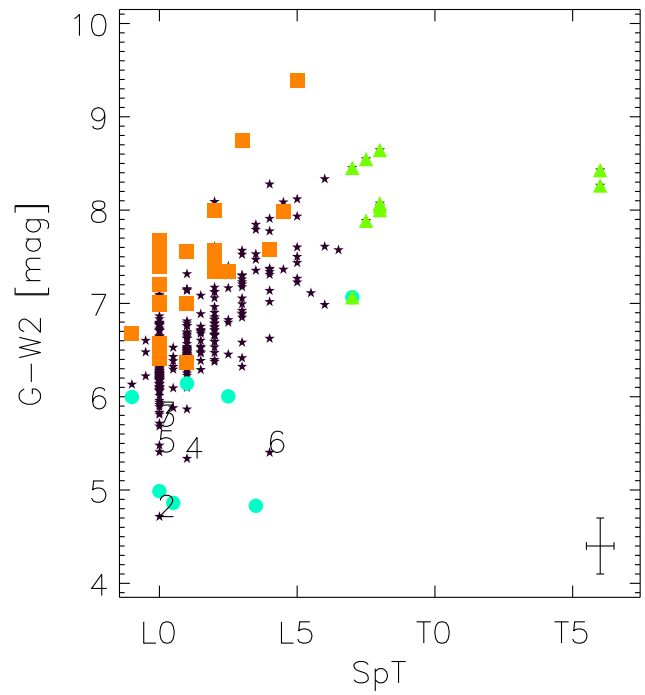

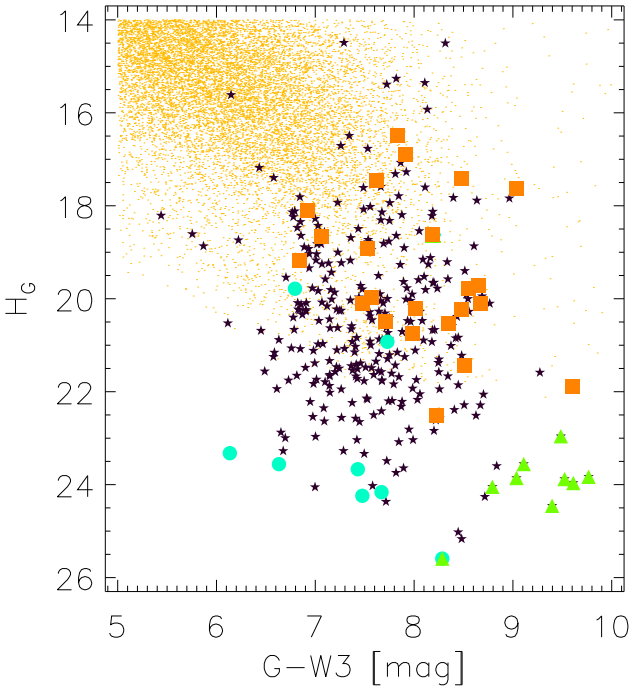

Figure 12. Colour–spectral type diagrams for $G - J$ and $G - W2$. Symbols have the same meaning as Fig. 11. The four outliers J0133−6314, J1245+4902, J1250+4418 and J1251+6243 are labelled 1–4, respectively. Additional colour–spectral type diagrams are found in Appendix A.

Figure 13. Colour–reduced proper motion H_G diagrams for $G - J$ and $G - W3$. Symbols have the same meaning as in Fig. 11. The top panel includes a significant part of the background objects, and the bottom panel is a zoom on the region with LT dwarfs. Additional colour–spectral type diagrams are found in Appendix A.

subdwarf (Scholz et al. 2009) and TWA 27 A is a member of the young TW Hya association (Gizis 2002) hence the outlier positions. Kelu-1 is a triple system, with Kelu-1 A, a spectroscopically identified L0.5+T7.5 (Stumpf et al. 2009) and Kelu-1 B, a L3pec dwarf 300 mas towards the southeast (Liu & Leggett 2005) of the primary double. *Gaia* should resolve and detect both the double primary system and the secondary so we assume that the object matched is the brighter Kelu-1 A. Indeed if we use the J magnitude of the combined system the object takes an outlier position in the absolute magnitude as a function of $G - J$ but not in absolute magnitude as a function of spectral type.

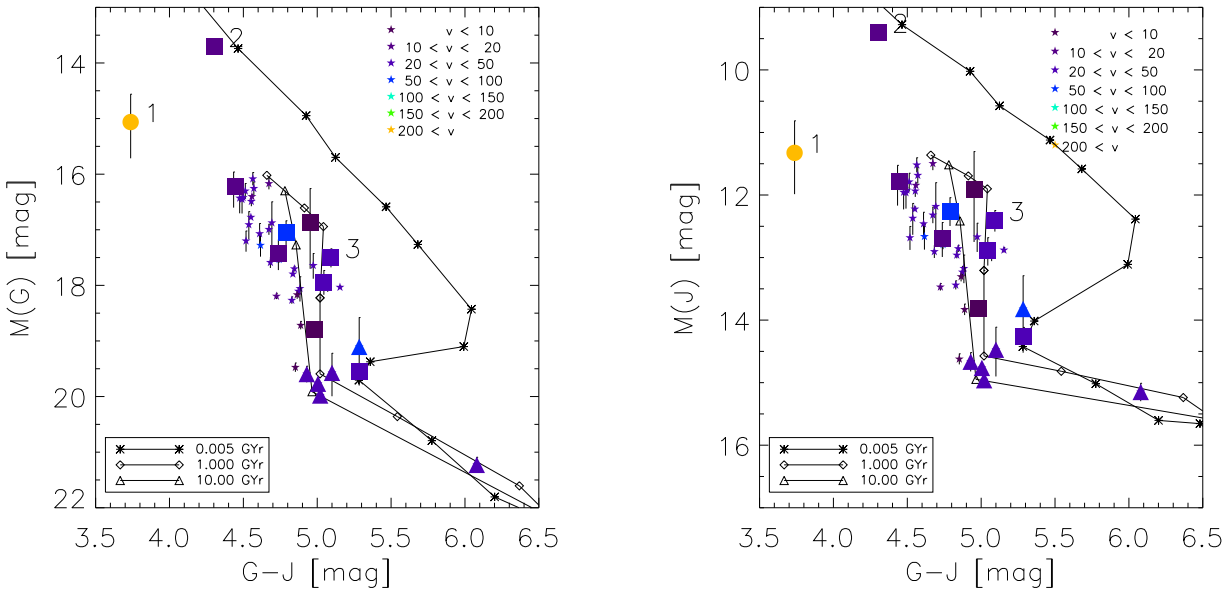

Figure 14. Absolute magnitude in G and J bands versus $G-J$. The colour of symbols indicates the velocity as given in the legend. Filled circles are subdwarfs, the squares are noted as young and triangles are objects later than L7, small stars are other L0−6 dwarfs. The objects labelled 1,2,3 are J1256−0224, TWA 27 A and Kelu-1 A, respectively.

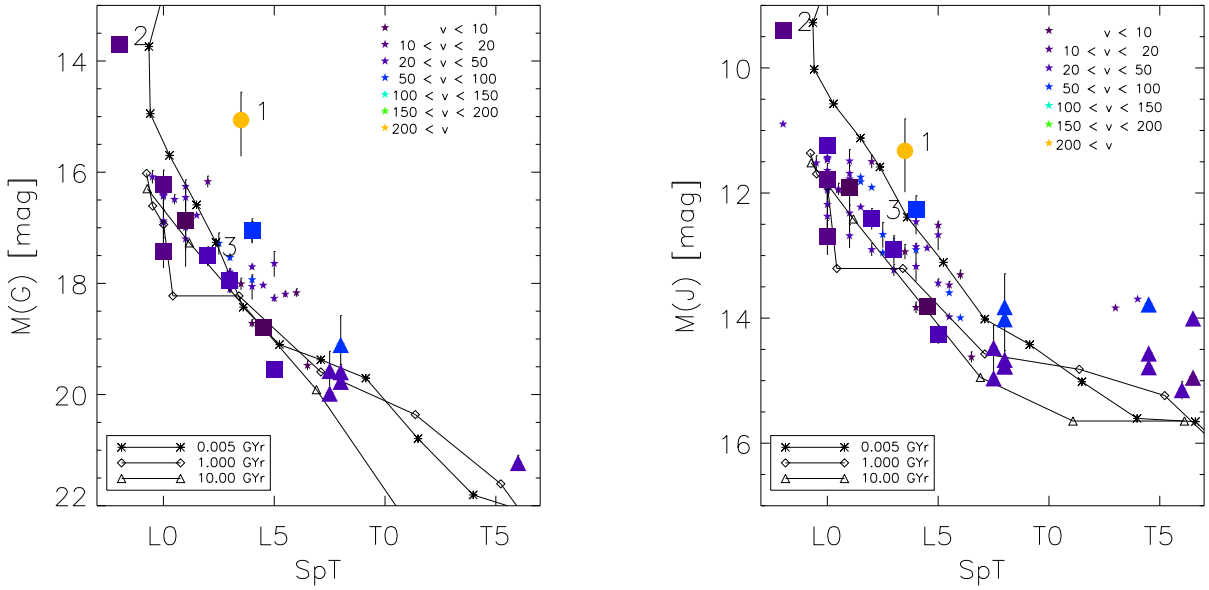

Figure 15. Absolute magnitude in G and J bands versus spectral types. The colour and shape of the symbols are as given in Fig. 14. The increased number of objects in the right panel are the LT dwarfs in CPM systems assuming the TGAS parallax which is only possible in this panel as we do not have G-band magnitudes for the CPM LT objects.

We have added the 28 CPM objects found in Section 4 to Fig. 15 with J-band magnitudes and adopting the parallax of the TGAS CPM companion. In some cases using the TGAS parallax is inappropriate, e.g. in systems that are unbound, but the consistency in the HR diagram indicates this is not a bad assumption. The fact that we can see differences, even in this small sample with heterogeneous parallaxes, is a taste of what to expect with the full GUCDS. The *Gaia* DR2 is expected to furnish precise parallaxes for most of the GUCDS and we will use the small differences in colour and absolute magnitude trends to find more direct indicators of age, metallicity and other physical properties.

6 CONCLUSIONS

We have produced a catalogue of all known LT dwarfs with estimates of their G magnitude and proper motions. We investigated 321 known LT dwarfs identified in the *Gaia* DR1. The number of LT dwarfs identified is in line with the expectation that *Gaia* will directly observe around 1000 LT dwarfs. The addition of new homogeneous optical magnitudes opens new possibilities for interpretation, and the addition of distances and proper motions directly from *Gaia* will allow hypothesis testing on a statistically significant sample size. In particular as we will be able to construct, for the first time, volume limited complete samples.

Table 8. Objects with $H_G > 24.0$.

Long name	Opt SpT	NIR SpT	H_G [mag]
ULAS J033350.84+001406.1	L0 sd[1]	L0 sd[2]	24.2
DENIS J081730.0−615520	...	T6[3]	24.9
2MASS 11555389+0559577	...	L7.5[4]	24.0
2MASS 11582077+0435014	L7 sd[5]	L7 sd[5]	25.6
SDSSp J120358.19+001550.3	L3[6]	L5[7]	24.4
2MASS 12074717+0244249	L8[8]	T0[9]	24.5
2MASS 12304562+2827583	...	L1[10]	24.3
ULAS J124425.90+102441.9	...	L0.5 sd[2]	24.2
2MASSW J1411175+393636	L1.5[11]	L1.5[7]	24.1
2MASSW J1515008+484742	L6[12]	L6[13]	25.2
2MASS 22114470+6856262	...	L2[5]	24.0
2MASS 22490917+3205489	L5[12]	...	25.0

Spectral type references: [1]Zhang et al. (2010), [2]Lodieu et al. (2012), [3]Artigau et al. (2010), [4]Knapp et al. (2004), [5]Kirkpatrick et al. (2010), [6]Fan et al. (2000), [7]Bardalez Gagliuffi et al. (2014), [8]Hawley et al. (2002), [9]Burgasser, Burrows & Kirkpatrick (2006b), [10]Sheppard & Cushing (2009), [11]Kirkpatrick et al. (2000), [12]Cruz et al. (2007), [13]Wilson et al. (2003).

The energy of LT dwarfs is primarily emitted in the near-infrared bands, and the energy being emitted in the *G* band is from the very red edge of the filter or is non-thermal. An example of non-thermal emission can be seen in the 1997 flare of 2MASSW J0149090+295613 which appears to have been for a short period brighter in the optical than it is in the infrared in its quiescent state (Liebert et al. 1999). *Gaia* in its normal operation will make an average of more than 80 observations per target with nine precise measures of *G* during each observation. This will be a well-defined, well-sampled data set that will be able to constraint and characterize the occurrences of flares in LT dwarfs in the optical regime.

Even though many of these objects will be close to the detection limit of *Gaia* their relative closeness and nominal *Gaia* precision will allow us to calculate tangential velocities with high precisions of metres-per-second. This precision will in turn allow us to co-locate them with local moving groups, streams and CPM systems that will provide a wealth of constraints on the physical properties of LT dwarfs. This is evidenced by the diverse locations of young and subdwarf LT objects.

We have found 15 candidate CPM systems by a comparison of our input catalogue to the *Gaia* TGAS subset. The ability to identify CPM pairs will allow us to push down towards the coolest brown dwarfs and the *Gaia* results will be crucial to fully characterize the systems and constrain objects that will be too faint for *Gaia*. Eventually, these benchmark GUCDS objects with age, metallicity and distance constraints provided by the brighter companion or by the parent association will be the sample to constrain our global picture of UCDs. Ultimately, we hope the GUCDS will allow us to identify observational spectral and colour indicators for the direct determination of physical properties like age and mass.

ACKNOWLEDGEMENTS

RLS's research was supported by a visiting professorship from the Leverhulme Trust (VP1-2015-063). FM, HRAJ and DJP acknowledge support from the UK's Science and Technology Facilities Council grant number ST/M001008/1. DB acknowledges support from the Spanish grant ESP2015-65712-C5-1-R. JAC acknowledges support from Spanish grant AYA2015-74551-JIN. JCB acknowledges program Comité Mixto ESO-Gobierno de Chile. The early work on this project was supported by the Marie Curie 7th European Community Framework Programme grant n.247593 *Interpretation and Parametrization of Extremely Red COOL dwarfs* (IPERCOOL) International Research Staff Exchange Scheme.

This research has made use of: observations collected at the European Organization for Astronomical Research in the Southern hemisphere under ESO programme 097.C-0592(A); data from the European Space Agency mission *Gaia*,[10] processed by the *Gaia* Data Processing and Analysis Consortium,[11] funded by national institutions participating in the *Gaia* Multilateral Agreement and in particular the support of ASI under contract I/058/10/0 (*Gaia* Mission – The Italian Participation to DPAC); the SIMBAD data base and the VizieR catalogue access tool, provided by CDS, Strasbourg, France; data products from the *Wide-field Infrared Survey Explorer*, which is a joint project of the University of California, Los Angeles, and the Jet Propulsion Laboratory/California Institute of Technology, and NEOWISE, which is a project of the Jet Propulsion Laboratory/California Institute of Technology; *WISE* and NEOWISE are funded by the National Aeronautics and Space Administration; the 2MASS, which is a joint project of the University of Massachusetts and the Infrared Processing and Analysis Center/California Institute of Technology, funded by the National Aeronautics and Space Administration and the National Science Foundation; the SpeX Prism Spectral Libraries, maintained by Adam Burgasser;[12] and the M, L, T and Y dwarf archives compendium maintained by Chris Gelino, Davy Kirkpatrick and Adam Burgasser.

REFERENCES

Ahn C. P. et al., 2014, ApJS, 211, 17
Allard F., Homeier D., Freytag B., 2013, Mem. Soc. Astron. Ital., 84, 1053
Artigau É., Radigan J., Folkes S., Jayawardhana R., Kurtev R., Lafrenière D., Doyon R., Borissova J., 2010, ApJ, 718, L38
Bailer-Jones C. A. L., 2015, PASP, 127, 994
Baraffe I., Chabrier G., Allard F., Hauschildt P. H., 2002, A&A, 382, 563
Bardalez Gagliuffi D. C. et al., 2014, ApJ, 794, 143
Belokurov V. A., Evans N. W., 2002, MNRAS, 331, 649
Burgasser A. J., Geballe T. R., Leggett S. K., Kirkpatrick J. D., Golimowski D. A., 2006a, ApJ, 637, 1067
Burgasser A. J., Burrows A., Kirkpatrick J. D., 2006b, ApJ, 639, 1095
Burgasser A. J. et al., 2015, AJ, 149, 104
Burrows A., Hubbard W. B., Lunine J. I., Liebert J., 2001, Rev. Modern Phys., 73, 719
Caballero J. A., 2009, A&A, 507, 251
Caballero J. A., 2014, Mem. Soc. Astron. Ital., 85, 757
Cruz K. L. et al., 2007, AJ, 133, 439
Cushing M. C., Rayner J. T., Vacca W. D., 2005, ApJ, 623, 1115
Cushing M. C. et al., 2011, ApJ, 743, 50
De Rosa R. J. et al., 2014, MNRAS, 445, 3694
Deacon N. R. et al., 2014, ApJ, 792, 119
Deacon N. R. et al., 2017, MNRAS, 467, 1126
Delfosse X. et al., 1997, A&A, 327, L25
Dhital S., West A. A., Stassun K. G., Schluns K. J., Massey A. P., 2015, AJ, 150, 57
Dieterich S. B., Henry T. J., Jao W.-C., Winters J. G., Hosey A. D., Riedel A. R., Subasavage J. P., 2014, AJ, 147, 94
Dupuy T. J., Liu M. C., 2012, ApJS, 201, 19
Elliott P., Bayo A., 2016, MNRAS, 459, 4499
Epchtein N. et al., 1999, A&A, 349, 236
Fabricius C. et al., 2016, A&A, 595, A3

[10] http://www.cosmos.esa.int/gaia
[11] http://www.cosmos.esa.int/web/gaia/dpac/consortium
[12] http://pono.ucsd.edu/~adam/browndwarfs/spexprism

Faherty J. K., Burgasser A. J., Cruz K. L., Shara M. M., Walter F. M., Gelino C. R., 2009, AJ, 137, 1
Faherty J. K. et al., 2016, ApJS, 225, 10
Fan X. et al., 2000, AJ, 119, 928
Folkes S. L. et al., 2012, MNRAS, 427, 3280
Gagné J., Lafrenière D., Doyon R., Malo L., Artigau É., 2014, ApJ, 783, 121
Gagné J. et al., 2015, ApJS, 219, 33
Gaia Collaboration et al., 2016a, A&A, 595, A1
Gaia Collaboration et al., 2016b, A&A, 595, A2
Gálvez-Ortiz M. C. et al., 2017, MNRAS, 466, 2983
Gauza B., Béjar V. J. S., Pérez-Garrido A., Zapatero Osorio M. R., Lodieu N., Rebolo R., Pallé E., Nowak G., 2015, ApJ, 804, 96
Gizis J. E., 2002, ApJ, 575, 484
Hawley S. L. et al., 2002, AJ, 123, 3409
Jiménez-Esteban F. M., Caballero J. A., Dorda R., Miles-Páez P. A., Solano E., 2012, A&A, 539, A86
Jones E. M., 1972, ApJ, 173, 671
Jones H. R. A., Steele I. A. eds, 2001, Ultracool Dwarfs: New Spectral Types L and T
Jordi C., 2012, Photometric Relationships between Gaia Photometry and Existing Photometric Systems Gaia Technical Note. Available at: http://www.rssd.esa.int/doc_fetch.php?id=2760608
Kirkpatrick J. D., 2005, ARA&A, 43, 195
Kirkpatrick J. D. et al., 1999, ApJ, 519, 802
Kirkpatrick J. D. et al., 2000, AJ, 120, 447
Kirkpatrick J. D. et al., 2008, ApJ, 689, 1295
Kirkpatrick J. D. et al., 2010, ApJS, 190, 100
Kirkpatrick J. D. et al., 2011, ApJS, 197, 19
Kirkpatrick J. D. et al., 2016, ApJS, 224, 36
Knapp G. R. et al., 2004, AJ, 127, 3553
Lépine S., Gaidos E., 2011, AJ, 142, 138
Liebert J., Kirkpatrick J. D., Reid I. N., Fisher M. D., 1999, ApJ, 519, 345
Lindegren L. et al., 2016, A&A, 595, A4
Littlefair S. P. et al., 2014, MNRAS, 445, 2106
Liu M. C., Leggett S. K., 2005, ApJ, 634, 616
Lodieu N., McCaughrean M. J., Barrado Y Navascués D., Bouvier J., Stauffer J. R., 2005a, A&A, 436, 853
Lodieu N., McCaughrean M. J., Barrado Y Navascués D., Bouvier J., Stauffer J. R., 2005b, A&A, 436, 853
Lodieu N. et al., 2007, MNRAS, 379, 1423
Lodieu N., Zapatero Osorio M. R., Rebolo R., Martín E. L., Hambly N. C., 2009, A&A, 505, 1115
Lodieu N., Espinoza Contreras M., Zapatero Osorio M. R., Solano E., Aberasturi M., Martín E. L., 2012, A&A, 542, A105
Ma B. et al., 2016, AJ, 152, 112
Mace G. N., 2014, PhD Thesis, Available at: http://www.astro.ucla.edu/~gmace/thesis.html
Mace G. N. et al., 2013, ApJ, 777, 36
Marocco F. et al., 2015, MNRAS, 449, 3651
Marocco F. et al., 2017, MNRAS, in press
Martín E. L., Basri G., Zapatero Osorio M. R., 1999, AJ, 118, 1005
Mason B. D., Wycoff G. L., Hartkopf W. I., Douglass G. G., Worley C. E., 2001, AJ, 122, 3466
Michalik D., Lindegren L., Hobbs D., 2015, A&A, 574, A115
Noll K. S., Geballe T. R., Leggett S. K., Marley M. S., 2000, ApJ, 541, L75
Oppenheimer B. R., Kulkarni S. R., Matthews K., van Kerkwijk M. H., 1998, ApJ, 502, 932
Pinfield D. J., Jones H. R. A., Lucas P. W., Kendall T. R., Folkes S. L., Day-Jones A. C., Chappelle R. J., Steele I. A., 2006, MNRAS, 368, 1281
Pope B., Martinache F., Tuthill P., 2013, ApJ, 767, 110
Proft S., Demleitner M., Wambsganss J., 2011, A&A, 536, A50
Ranc C., Cassan A., 2014, in Ballet J., Martins F., Bournaud F., Monier R., Reylé C., eds, SF2A-2014: Proc. Annual Meeting of the French Society of Astronomy and Astrophysics. p. 269
Reid I. N., Cruz K. L., Kirkpatrick J. D., Allen P. R., Mungall F., Liebert J., Lowrance P., Sweet A., 2008, AJ, 136, 1290
Riedel A. R., Blunt S. C., Lambrides E. L., Rice E. L., Cruz K. L., Faherty J. K., 2017, AJ, 153, 95
Sahu K. C., Bond H. E., Anderson J., Dominik M., 2014, ApJ, 782, 89
Sarro L. M., Berihuete A., Carrión C., Barrado D., Cruz P., Isasi Y., 2013, A&A, 550, A44
Schmidt S. J., West A. A., Hawley S. L., Pineda J. S., 2010, AJ, 139, 1808
Scholz R.-D., 2016, A&A, 587, A51
Scholz R.-D., Storm J., Knapp G. R., Zinnecker H., 2009, A&A, 494, 949
Sheppard S. S., Cushing M. C., 2009, AJ, 137, 304
Skrutskie M. F. et al., 2006, AJ, 131, 1163
Skrzypek N., Warren S. J., Faherty J. K., 2016, A&A, 589, A49
Smart R. L., 2014, Mem. Soc. Astron. Ital., 85, 649
Smith L. et al., 2014, MNRAS, 443, 2327
Smith L. C. et al., 2015, MNRAS, 454, 4476
Sozzetti A., Giacobbe P., Lattanzi M. G., Micela G., Morbidelli R., Tinetti G., 2014, MNRAS, 437, 497
Stumpf M. B., Brandner W., Köhler R., Bouy H., Henning T., 2009, AIPC, 1094, 561
Tabernero H. M., Montes D., González Hernández J. I., 2012, A&A, 547, A13
Thompson M. A. et al., 2013, PASP, 125, 809
Veras D., 2016, MNRAS, 463, 2958
West A. A., Hawley S. L., Bochanski J. J., Covey K. R., Reid I. N., Dhital S., Hilton E. J., Masuda M., 2008, AJ, 135, 785
West A. A. et al., 2011, AJ, 141, 97
Wilson J. C., Miller N. A., Gizis J. E., Skrutskie M. F., Houck J. R., Kirkpatrick J. D., Burgasser A. J., Monet D. G., 2003, in Martín E., ed., IAUS, 211, 197 pub. ASP
Wright E. L. et al., 2010, AJ, 140, 1868
Yip A. K. P., Pinfield D. J., Kurtev R., Gromadzki M., Marocco F., 2016, in 19th Cambridge Workshop on Cool Stars, Stellar Systems, and the Sun, 137, pub. Zenodo
York D. G. et al., 2000, AJ, 120, 1579
Zapatero Osorio M. R., Rebolo R., Bihain G., Béjar V. J. S., Caballero J. A., Álvarez C., 2010, ApJ, 715, 1408
Zhang Z. H. et al., 2009, A&A, 497, 619
Zhang Z. H. et al., 2010, MNRAS, 404, 1817

SUPPORTING INFORMATION

Supplementary data are available at *MNRAS* online.

Table 2. The GUCDS input catalogue.
Table 4. New parameters for the GUCDS-DR1 catalogue.
Table 5. The common-distance, common-proper-motion pair candidates identified here.

This paper has been typeset from a TEX/LATEX file prepared by the author.